Molecular Therapy
Methods & Clinical Development
Original Article

Use of Nanovesicles from Orange Juice to Reverse Diet-Induced Gut Modifications in Diet-Induced Obese Mice

Emmanuelle Berger,[1] Pascal Colosetti,[1,6] Audrey Jalabert,[1,6] Emmanuelle Meugnier,[1] Oscar P.B. Wiklander,[2] Juliette Jouhet,[3] Elisabeth Errazurig-Cerda,[4] Stéphanie Chanon,[1] Dhanu Gupta,[2] Gilles J.P. Rautureau,[5] Alain Geloen,[1] Samir El-Andaloussi,[2] Baptiste Panthu,[1] Jennifer Rieusset,[1] and Sophie Rome[1]

[1]CarMeN Laboratory (INRAe U1397, INSERM U1060, Lyon 1 University, INSA Lyon), Bâtiment CENS ELI-2D, Pierre-Bénite, France; [2]Department of Laboratory Medicine, Division of Biomolecular and Cellular Medicine, Karolinska Institutet, 141 57 Huddinge, Sweden; [3]Laboratoire de Physiologie Cellulaire & Végétale (LPCV), CNRS (UMR5168)/Université Grenoble Alpes/INRAe (UMR1417)/CEA Grenoble, Institut de Biosciences et Biotechnologies de Grenoble, France; [4]Centre d'Imagerie Quantitative Lyon Est (CIQLE), Rockefeller Faculty of Medicine, Lyon, France; [5]Université de Lyon, CNRS, Université Claude Bernard Lyon 1, ENS de Lyon, Centre de RMN à Très Hauts Champs (CRMN), FRE 2034, Villeurbanne, France

We have determined whether orange juice-derived nanovesicles (ONVs) could be used for the treatment of obesity-associated intestinal complications. ONVs were characterized by lipidomic, metabolomic, electron microscopy. *In vitro*, intestinal barriers (IBs = Caco-2+HT-29-MTX) were treated with ONVs and co-cultured with adipocytes to monitor IB fat release. *In vivo*, obesity was induced with a high-fat, high-sucrose diet (HFHSD mice) for 12 weeks. Then, half of HFHSD mice were gavaged with ONVs. One-month ONV treatment did not modify HFHSD-induced insulin resistance but reversed diet-induced gut modifications. In the jejunum, ONVs increased villi size, reduced triglyceride content, and modulated mRNA levels of genes involved in immune response (tumor necrosis factor [TNF]-α and interleukin [IL]-1β), barrier permeability (CLDN1, OCLN, ZO1), fat absorption, and chylomicron release. ONVs targeted microsomal triglyceride transfer protein (MTP) and angiopoietin-like protein-4 (ANGPTL4), two therapeutic targets to reduce plasma lipids and inflammation in gastrointestinal diseases. Interestingly, ONV treatment did not aggravate liver steatosis, as MTP mRNA was increased in the liver. Therefore, ONVs protected both intestine and the liver from fat overload associated with the HFHSD. As ONVs concentrated amino acids and bioactive lipids versus orange juice, which are deficient in obese patients, the use of ONVs as a dietary supplement could bring physiological relevant compounds in the jejunum to accelerate the restoration of intestinal functions during weight loss in obese patients.

INTRODUCTION

The identification of active constituents from our diet is an important step to understand the impact of diet on health and disease development and for the formulation of functional foods and nutraceuticals. No diet has been proven to cure cancer or metabolic diseases, but plant-based diets may benefit treatment. In that context, it was found that in addition to vitamins, sterols, polyphenols, and fibers, plants also contained nanovesicles with interesting biological properties on the digestive tract.[1] Similar to mammalian cells, plant cells export proteins, lipids, and nucleic acids into the extracellular space inside nanosized vesicles, such as exosomes.[2–4] Exosome are synthesized inside the cells, from the endosomal pathway in which intraluminal vesicles progressively accumulate during endosome maturation. Exosomes are released into the extracellular space through exocytosis, and in plants exosome secretion is enhanced in response to bacterial/parasite infections.[5,6] They contain proteins related to biotic and abiotic stresses, suggesting that these nanovesicles would play a vital role in basal immunity and responses to environmental stresses in plants. Studies based on *in vitro* models with cell cultures or gavage of mice with fruit-derived nanovesicles have demonstrated that they have anti-inflammatory (e.g., protect against colitis injury[7,8]) and anti-oxidant properties. It has been demonstrated that the beneficial effects of fruit-derived nanovesicles could be used as additional strategies in cancer treatment in association with chemotherapies.[9] Other data suggested that they could mitigate the immune response induced by injuries in the intestinal barrier (IB) challenged with chemical compounds.[10] Their actions might not be restricted to intestine, as they are also able to inhibit alcohol-induced reactive oxygen species (ROS) production in the liver during alcohol-induced liver damage.[11] From a nutritional point of view, fruit-derived nanovesicles are composed of fruit-derived lipids and proteins that are absorbed by the IB, similar to other food components, when they are given per os.[11–14] However, there are presently no data on their metabolic properties on enterocytes which might potentialize

Received 3 June 2020; accepted 10 August 2020;
https://doi.org/10.1016/j.omtm.2020.08.009.

[6]These authors contributed equally to this work.

Correspondence: Sophie Rome, CarMeN Laboratory (INRAe U1397, INSERM U1060, Lyon 1 University, INSA Lyon), Bâtiment CENS ELI-2D, Pierre-Bénite, France.
E-mail: srome@univ-lyon1.fr

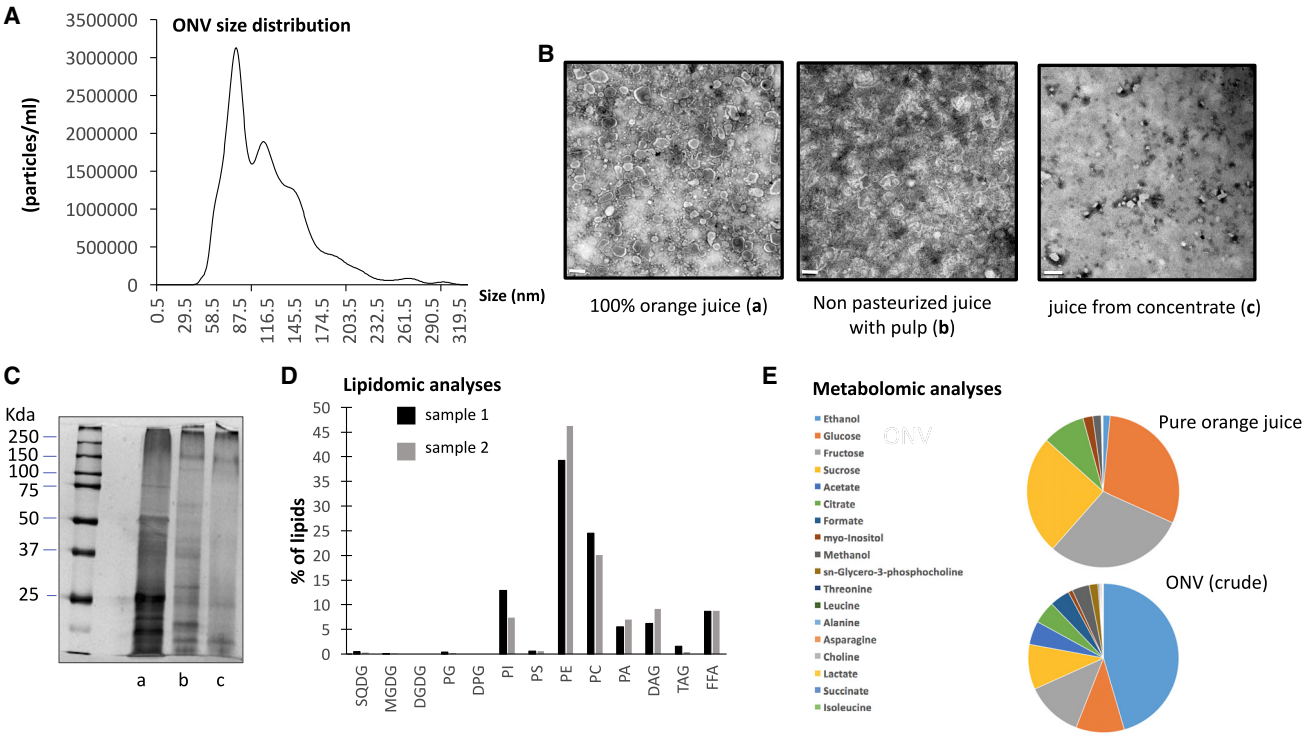

Figure 1. Characterization of ONVs

(A) ONV pellet size distribution isolated from pure orange juice, by nanoparticle tracking analyses. (B) TEM of ONV pellets extracted from different preparations of orange juices (scale bars, 200 nm for a and b, or 500 nm for c). (C) Polyacrylamide gel of ONV proteins detected with silver staining (a, pure juice; b, unpasteurized juice; c, reconstituted from concentrated juice). (D) Lipids identified in 1 mg of ONV pellet expressed as percentage of total lipids. The two colors represent two lipidomic analyses from two ONV preparations. SQDG, sulfoquinovosyl diacylglycerol; MGDG, monogalactosyldiacylglycerol, DGDG, digalactosyldiacylglycerol, PG, phosphatidylglycerol; DPG, diphosphatidylglycerol (or cardiolipin); PI, phosphatidylinositol; PS, phosphatidylserine; PE, phosphatidylethanolamine; PC, phosphatidylcholine; PA, phosphatidic acid; DAG, diacylglycerol; TAG, triacylglycerol; FFA, free fatty acids. Full lipid composition is indicated in Figure S2. (E) Metabolites found in orange juice or ONVs identified by proton nuclear magnetic resonance. Data are expressed as % of total for each condition. The full metabolomic data are provided in Table S1. Only metabolites from crude ONVs are shown because they were prepared using the same conditions as for pure orange juice.

or decrease the bioactive effects of drugs when these fruit-derived nanovesicles are used for drug delivery.[15] As fruit consumption is beneficial for human health and is considered in preventive medicine, it is important to determine whether fruit-derived nanovesicles could participate in these properties and could be used as nutritional strategies for the treatment of metabolic complications associated with obesity (e.g., dyslipidemia, hyperglycemia, insulin resistance, increased intestinal permeability). In this context, 100% orange juice (from *Citrus sinensis* (L.) Osbeck) contains many elements that can reduce the risk of heart disease and cardiac arrhythmias, lower blood pressure, balance cholesterol, and reduce the occurrence of many types of cancers.[16–21] Orange juice also has antioxidant and anti-inflammatory properties that can be used for the treatment of intestinal inflammatory diseases that cause excessive tissue injury and affect mucosal integrity.[22–25] Orange juice consumption can also accelerate the recovery of the villous architecture and intestinal permeability after a surgical stress.[26] From a nutritional point of view, 100% orange juice intake has been associated with better diet quality in children and adults. However, the high quantity of sugars and its acid pH are matters of debate for its consumption by metabolically perturbed populations. Therefore, in this study we have characterized orange juice-derived nanovesicles (ONVs) and determined whether these have the potential to restore intestinal functions altered in a model of diet-induced obesity in mice. This is the first study on the nutritional action of plant-derived nanovesicles. Our data demonstrate that ONVs, and likely all nanovesicles derived from edible plants, concentrate plant species-specific lipids and metabolites that are captured by the IB and consequently modulate lipid metabolism at whole-body level. This has to be taken into account in studies using plant-derived nanovesicles for drug delivery, as it might interfere or potentialize drug biological actions.

RESULTS

Isolation and Characterization of ONVs

ONVs were isolated by differential centrifugations and filtration steps from 100% fruit juice (Figure S1). Nanosight analysis showed a polydispersed population of vesicles (Figure 1A) with a negative zeta potential of −18.23 ± 2.7mV. ONV heterogeneity was confirmed by electron microscopy (Figure 1B) showing small vesicles (<50 nm) and large vesicles (>150 nm) that could be separated by size-exclusion chromatography (Figures S1C and S1D). Conversely, to what is

usually observed, the small vesicles eluated before the large one, suggesting that the large vesicles could be richer in lipids and thus less dense than the small vesicles. As the population of ONVs was very polydispersed, it was not possible to measure the concentration of the vesicles based on their size distributions. Thus, we have measured the concentration of proteins contained in the ONV pellet. Around 1 mg of ONV equivalent protein per 350 mL of juice was obtained. We tested their biological actions on Caco-2 cells by monitoring changes in cell index during 22 h. All vesicular populations (ONVs, large, small) increased significantly the cell index of Caco-2 cells versus untreated Caco-2 cells, suggesting similar effects on recipient cells after 22 h (Figure S1F). Therefore, considering that drinking orange juice is associated with the consumption of the whole population of vesicles, we have decided to consider the whole-ONV pellet in this study. We then have determined whether industrial processes could alter the quantity or quality of ONVs. We extracted ONVs from different industrial juices by using the same starting volume. When pulp (juice sacs) was preserved during the process, ONVs were still visible by transmission electron microscopy (TEM), but their morphology was strongly altered (Figure 1B). When juice was obtained from concentrated orange juice no ONVs were detected (Figure 1B). Protein profiling confirmed this result and also showed an alteration of protein content in the preparation of ONVs from industrial juices (Figure 1C). Therefore, these data indicated that ONVs were lost in industrial preparations that removed the juice sacs.

Lipidomic and Metabolomic Profiles of ONVs

As the purpose of this study was to determine the function of ONVs on the metabolism of high-fat, high-sucrose diet (HFHSD) mice, the lipid composition associated with these lipid-derived vesicles was first assessed (Figure 1D). Lipidomic analyses on two independent preparations showed that ONVs contained phosphatidylethanolamine (PE) (~40%), phosphatidylcholine (PC) (~25%), phosphatidylinositol (PI), (~12%) and phosphatidic acid (PA) (~5%). In particular, PE (34:2) and PC (34:2)-(36:2)-(36:3) were highly represented (Figure S2). ONVs also contained diacylglycerol (DAG) and free fatty acids (FFAs), mainly palmitic acid (C16:0), oleic acid (C18:1), linoleic acid (C18:2), and α-linolenic acid (C18:3). Compared to previous lipidomic analyses, the ONV lipid profile was very similar to grapefruit-derived nanovesicles,[27] suggesting that Rutaceae family-derived nanovesicles have a specific lipid composition, in particular their PE/PA ratio is reversed versus grape- or ginger-derived vesicles.[10,14] Proton nuclear magnetic resonance (^{1}H-NMR) showed that ONVs did not contain vitamin C and naringenin, which are major active compounds of orange juice (Table S1). ONVs contained carbohydrates (glucose, fructose, sucrose) and amino acids (alanine, asparagine isoleucine, threonine, leucine). ONVs accumulated leucine, threonine, formate, methanol, ethanol, and *sn*-glycero-3-phosphocholine versus orange juice (Figure 1E).

In Vivo Biodistribution of ONVs and ONV Uptake by IBs *In Vitro*

To investigate whether ONVs were internalized by human cells, IBs were incubated with ONVs labeled with lipophilic dye PKH67. Fluorescent cells were detected already after 3 h (Figure 2A), indicating that ONVs could penetrate rapidly in IBs. ONV uptake was not inhibited by cytochalasin D, known as a macropinocytosis inhibitor, but it was significantly reduced in the presence of caveolae-mediated endocytosis inhibitor indomethacin (Figures 2B and 2C). In order to determine the biodistribution of ONVs during digestion, mice were gavaged with 150 μg of labeled ONVs, and ONV fluorescence distribution was determined in metabolic organs after 6 h. Fluorescence was detected in the gut only and not in other tissues (Figure 2D). In the gut, there was a gradient of fluorescence from the jejunum-ileum to the cecum-ascending colon (Figure 2E).

ONVs Induced the Release of Chylomicron-Associated Triglycerides (TGs) from IBs *In Vitro*

As shown in Figure S3, 10 μg versus 1 μg of ONV addition to the cell culture induced ROS production (Figures S3A and S3B) associated with IB cell death, showing a toxicity of ONVs at high concentrations (Figures S3B and S3C). Therefore, we used 1 μg/mL ONVs to treat differentiated IBs. Soon after 3 h of treatment, we observed a strong decrease in TG levels in ONV-treated IBs versus control IBs (Figures 3A and 3B). Then, the growth medium was renewed and ONV-treated IBs were co-cultured in the presence of differentiated adipocytes. After 24 h of co-culture, we detected a significant increase in lipid droplet size in adipocytes co-cultured with ONV treated IBs versus untreated IBs (Figure 3C). In addition, TG levels were increased in adipocytes (Figures 3D and 3E). Lipid accumulation in adipocytes induced changes in their morphology and a loss of cell adhesion force. As a result, the cell index decreased as observed in Figure 3F. These data indicated that OVNs induced the release of chylomicron-associated TGs from IBs, which were further hydrolyzed and stored as TGs in adipocytes. These results were independent of glucose concentration in culture medium (data not shown). Gene expressions analyses (Table S2A) also suggested that IBs+ONVs absorbed less fatty acids (i.e., decreased FABP1/2 mRNAs) and had increased levels of fatty oxidation (i.e., increased PGC1α mRNA), which might contribute to the TG depletion in ONV-treated IBs versus untreated IBs.

ONVs Modulated Jejunum Morphology and mRNA Levels of Genes Involved in Permeability

As ONVs had an effect on IB TG disposal *in vitro*, we speculated that they might have functional properties on the intestine *in vivo*, as shown for other plant-derived nanovesicles.[1] We validated this hypothesis by using HFHSD mice. As shown on Figures S4A and S4B, HFHSD mice were glucose-intolerant and insulin-resistant after 12 weeks of an HFHSD, based on both glucose tolerance tests (GTTs) and insulin tolerance tests (ITTs). Four-week treatment with ONVs neither restored significantly these metabolic alterations (Figures S4C–S4E) nor modified body weight level, adipose tissue, or liver mass (Figures S3H and S3I). HFHSD mice had a significant decrease in cecum weight versus standard diet (SD) mice (Figure 4A). Conversely, the lengths of colon and small intestine were not affected by the diet (Figures 4B and 4C). These three parameters were not modified in HFHSD+ONV mice, suggesting no global effect on the intestine. As fluorescent ONVs accumulated mainly in the jejunum (Figure 2E), we focused on this region. The treatment with ONVs

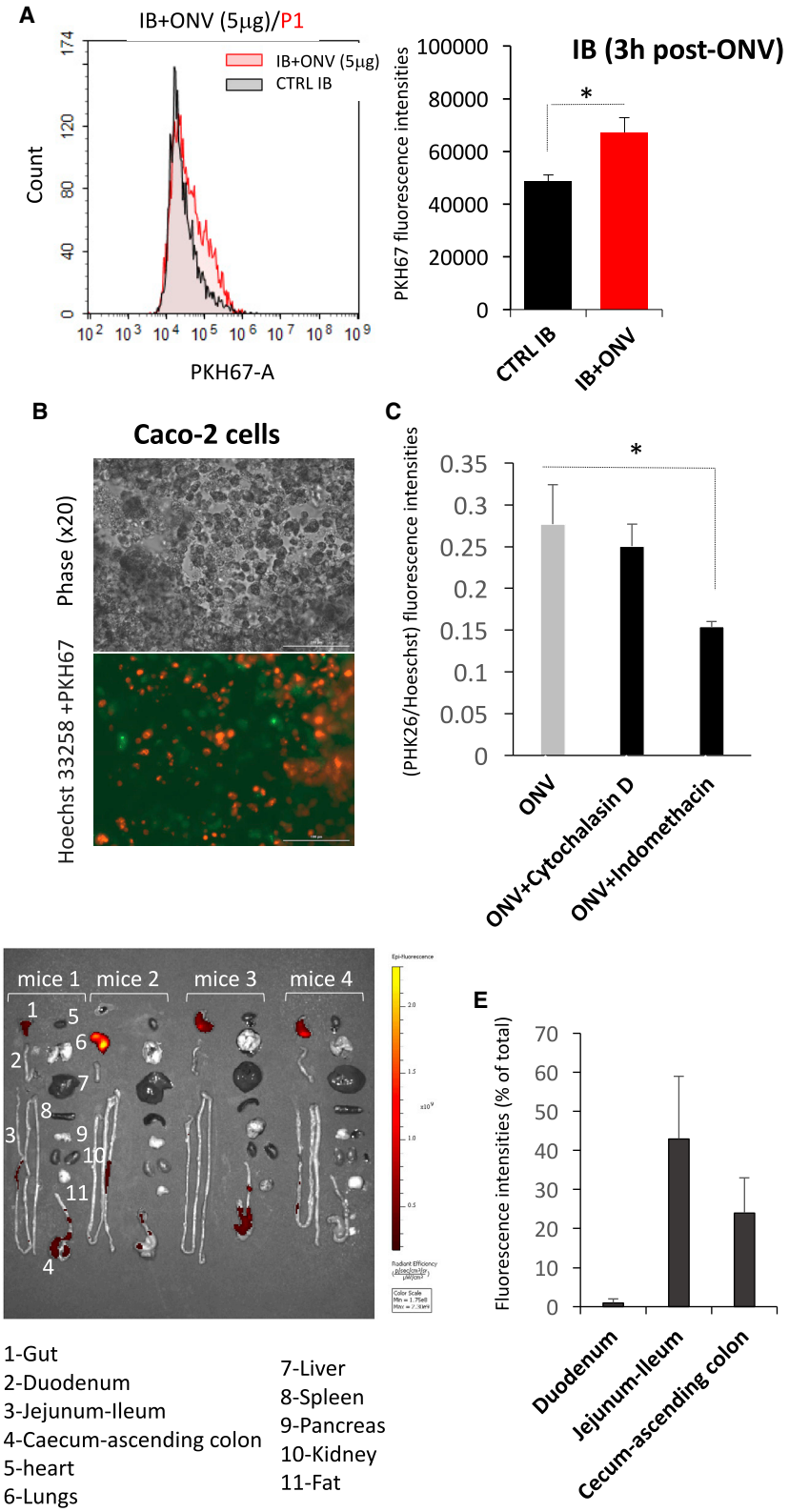

Figure 2. ONV Intestinal Biodistribution and Cellular Absorption

(A) Quantification of PKH67 fluorescence in IBs after ONV treatment (5 µg/mL, 3 h). Cells were trypsinated and PKH67 fluorescent cells were sorted by flow cytometry. Data are presented as mean PKH67 fluorescence intensity ± SEM (n = 3). *$p < 0.05$ (Student's t test, versus untreated IBs). (B) Representative images of Caco-2 cells treated with 10 µg of PKH67-labeled ONVs, 3 h post-treatment. Cell nuclei were labeled with Hoechst 33258. (C) Caco-2 cells were pre-treated with inhibitors of endocytosis and treated with PKH26-labeled ONVs. Fluorescence intensities of either PKH26 or Hoechst 33258 were quantified with a Cytation 3 cell imaging reader. Data are mean ratios of fluorescence intensities (PKH26/Hoechst 33258; n = 4 replicates). (D) IVIS images, 6 h post-gavage with 100 µg of DIR-labeled ONVs. (E) *In vivo* biodistribution of the fluorescence from DIR-ONVs in the digestive tract of SD mice 6 h post-gavage, normalized to background (n = 3 PBS-DIR as control background of DIR fluorescence, and n = 4 DIR-labeled ONV gavaged mice).

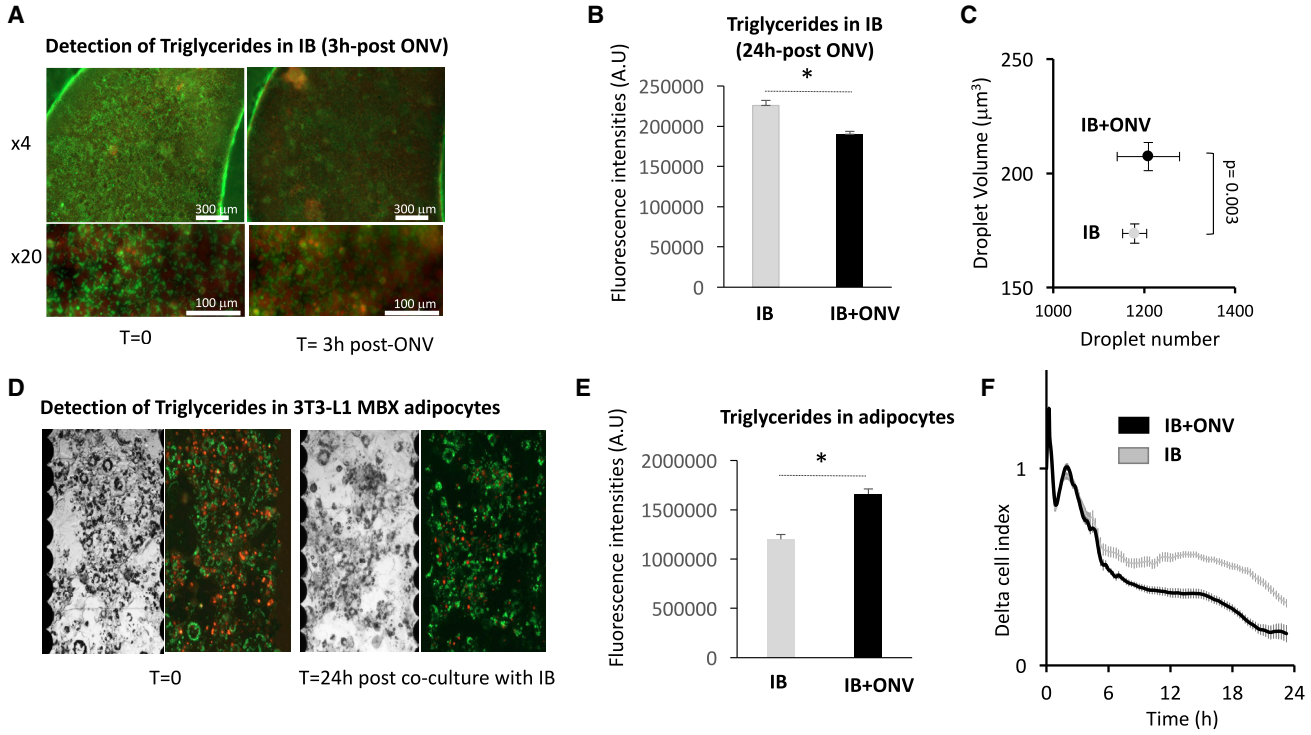

Figure 3. ONV Effects on Caco-2/HT29-MTX Intestinal Barrier

(A) Representative images of IBs obtained with identical image acquisition parameters for AdipoRed and Hoechst 33258 on a Cytation 3 platform, showing the decrease in TG content post-treatment with ONV (3 h, 1 µg/mL) (objective ×4, IBs grown in 96-well inserts; objective ×20, IBs grown in six-well inserts). (B) TG levels in IBs 24 h post-treatment with ONVs, measured by quantification of AdipoRed fluorescence intensities in IB cells sorted by flow cytometry (n = 3). (C) Volume and number of lipid droplets in 3T3-L1 MBX differentiated adipocytes co-cultured with ONV-pretreated IBs (n = 6–12 replicates). (D) Representative images of 3T3-L1 MBX differentiated adipocytes in 96-well E-plates after 24 h of co-culture with IBs. Contrast phase (left panels) and corresponding merged AdipoRed-Hoechst 33258 (right panels) are shown. (E) TGs in adipocytes. Data are mean ratios of fluorescence intensities (AdipoRed-Hoescht 33258, n = 12 replicates) quantified with a Cytation 3 cell imaging reader. (F) xCELLigence analyses of 3T3-L1 MBX differentiated adipocytes, co-cultured with ONV-pretreated IBs during 24 h. The data represent real-time monitoring of 3T3-L1 MBX cell index normalized to the cell index at T = 0 (mean delta cell index, every 5 min during 50 cycles, then every 15 min) for 22 h. The decrease of cell index in the 3T3-L1 MBX + pre-treated IBs versus 3T3-L1 MBX + control IBs indicated a decrease in adipocyte adherence due to lipid accumulation.[28] *$p < 0.05$, student t test.

induced an increase in villi size in HFHSD jejunum (Figures 4D and 4E), indicating that these lipid-derived nanovesicles lead to an increase in absorptive area. Of note, no modifications of villi or crypt sizes were observed for the other parts of the intestine (data not shown), suggesting that this result was specific for the jejunum. As it was previously demonstrated that HFHSD consumption induced intestinal permeability,[29] we also quantified the expression of genes coding for proteins located in the tight junctions in jejunum. HFHSD+ONV mice had increased mRNA levels of CLDN1, OCLN, and ZO1 compared with HFHSD mice. These data suggest that ONVs could modulate intestinal permeability (Table S2B). Associated with the onset of intestinal permeability, it is known that an HFHSD causes a deficiency within the intestinal immune system leading to the colonization of the epithelium by gut bacteria.[30] In agreement, mRNA levels of tumor necrosis factor (TNF)-α and interleukin (IL)-1β, released from immune cells, were decreased in jejunum from HFHSD versus SD mice, whereas the expression of Toll-like receptor 4 (TLR4), required to maintain intestinal homeostasis and to limit bacterial infiltration,[31] was not differentially expressed. Gavage with ONVs reversed TNF-α and IL-1β mRNA levels and induced the expression of TLR4 in the jejunum of HFHSD+ONV versus HFHSD mice (Table S2B), suggesting a possible restoration of the intestinal immune system.[32]

ONVs Modulated the Expressions of Genes Involved in Lipid Absorption and Release in Jejunum and Liver of HFHSD Mice

We quantified the levels of TGs in the jejunum of each group of mice as a reflection of intestinal lipid absorption and release. TG content did not change in the jejunum of HFHSD versus SD mice (Figure 4F), but it increased in blood and liver of HFHSD versus SD mice (Figure 4G; Figure S4I). ONV consumption triggered a decrease in TG content in the jejunum of HFHSD+ONV versus HFHSD mice at the fasted state (Figure 4F), confirming the data obtained with the IBs *in vitro* (Figures 3A and 3B). In order to explain the decrease in jejunum TG content in HFHSD+ONV mice, we quantified the expression of genes involved in lipid absorption and metabolism of enterocytes. The mRNA levels of ABCG5, ABCG8, FABP2, and FABP4 were neither affected by the diet nor by ONV

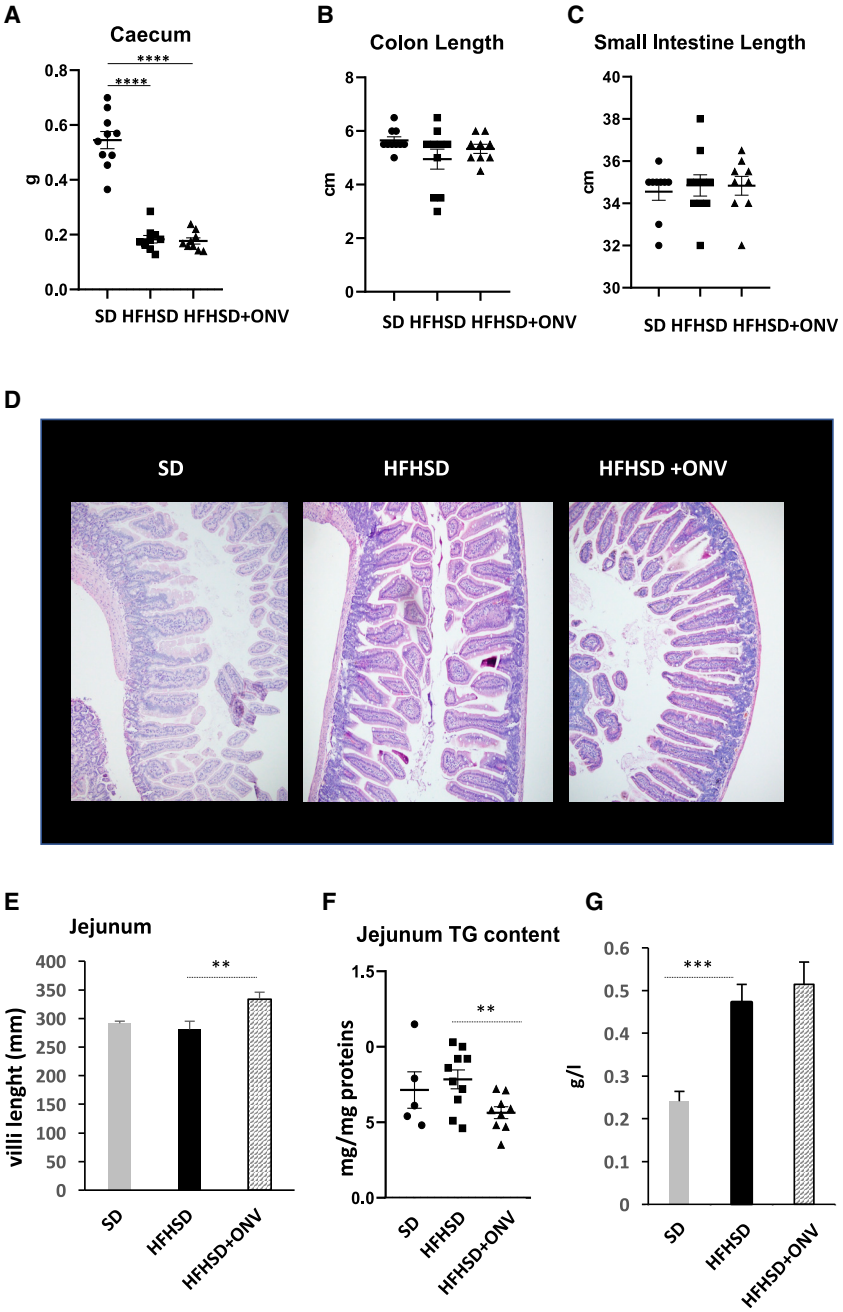

Figure 4. ONV Effects on Jejunum Morphology and TG Content

(A) Cecum weight (g) (n = 10). (B) Size of the colon (cm) (n = 10). (C) Size of the intestine (cm) (n = 10). (D) Representative images of the jejunum used to quantify the size of the villi (hematoxylin and eosin staining). (E) Villi length in the jejunum (n = 5). (F) TG levels in the jejunum per gram of proteins (SD, n = 5; HFHSD, n = 10; HFHSD+ONV, n = 10). (G) Plasma TG levels. SD, standard diet; HFHSD, high-fat, high-sucrose diet; HFHSD+ONV, HFHSD mice gavaged with ONVs.

supplementation (Table S2B). Conversely, mRNA levels of APOB, CD36, DGAT1, L-FABP, I-FABP, FATP4, and microsomal TG transfer protein (MTP) were increased whereas those of SR-B1, ATGL, angiopoietin-like protein-4 (ANGPTL4), NPC1L1, and ACAT2 were decreased in HFHSD versus SD mice (Table S2B). These data, summarized in Figure 5, showed that consumption of an HFHSD induced fatty acid absorption, an increase in TG synthesis, and thus chylomicron synthesis and release. Among the HFHSD mice, those fed with ONVs for 4 weeks had increased expressions of ACAT2, ANGPTL4, and DGAT1, but decreased expression of FABP2, FATP4, and MTP versus HFHSD animals. These data indicated that syntheses of TGs and prechylomicron were strongly reduced in HFHSD+ONV versus HFHSD mice. In addition, jejunum harvested fewer lipids from ingested food (i.e., increased expression of ANGPTL4[33]), and thus fat absorption was also reduced. TG decrease in jejunum of HFHSD+ONV mice was not associated with modifications of blood TGs (Figure 4G).

In order to determine whether reduced jejunum TG content affected whole-body TG homeostasis, we performed an oral lipid tolerance test and followed the modulations of TG concentrations in plasma. Plasmatic TG normalization level following administration of a lipid bolus provides integrated information about enteric lipid absorption, lipid packaging into chylomicrons, and liver TG clearance and release. As expected, SD mice displayed lower post-prandial TG excursion compared with dyslipidemic HFHSD or HFHSD+ONV mice (Figures 6A and 6B). Mice fed with HFHSD+ONV displayed higher post-prandial plasma TG levels versus HFHSD at 2 h, but not at 4 h (Figure 6A), indicating that plasma TG clearance was not modified by ONVs. However, during 4 h HFHSD+ONV mice had higher plasma TG concentrations than did HFHSD mice (Figure 6B). As enteric lipid absorption and TG release were reduced in HFHSD+ONV versus HFHSD mice, the increase of plasma TG after lipid bolus was likely due to a higher release of TG-rich lipoprotein by the liver. Indeed, HFHSD+ONV mice had an increased MTP mRNA level in liver required for very-low-density lipoprotein (VLDL) biosynthesis without modification of CD36 mRNA expression, involved in lipid uptake (Table S2B). In agreement, we observed a small, but not significant, decrease in liver mass (Figure S3I) and in liver TG content (Figure 6C) in HFHSD+ONV versus HFHSD mice. These were not sufficient to detect a clear amelioration of liver

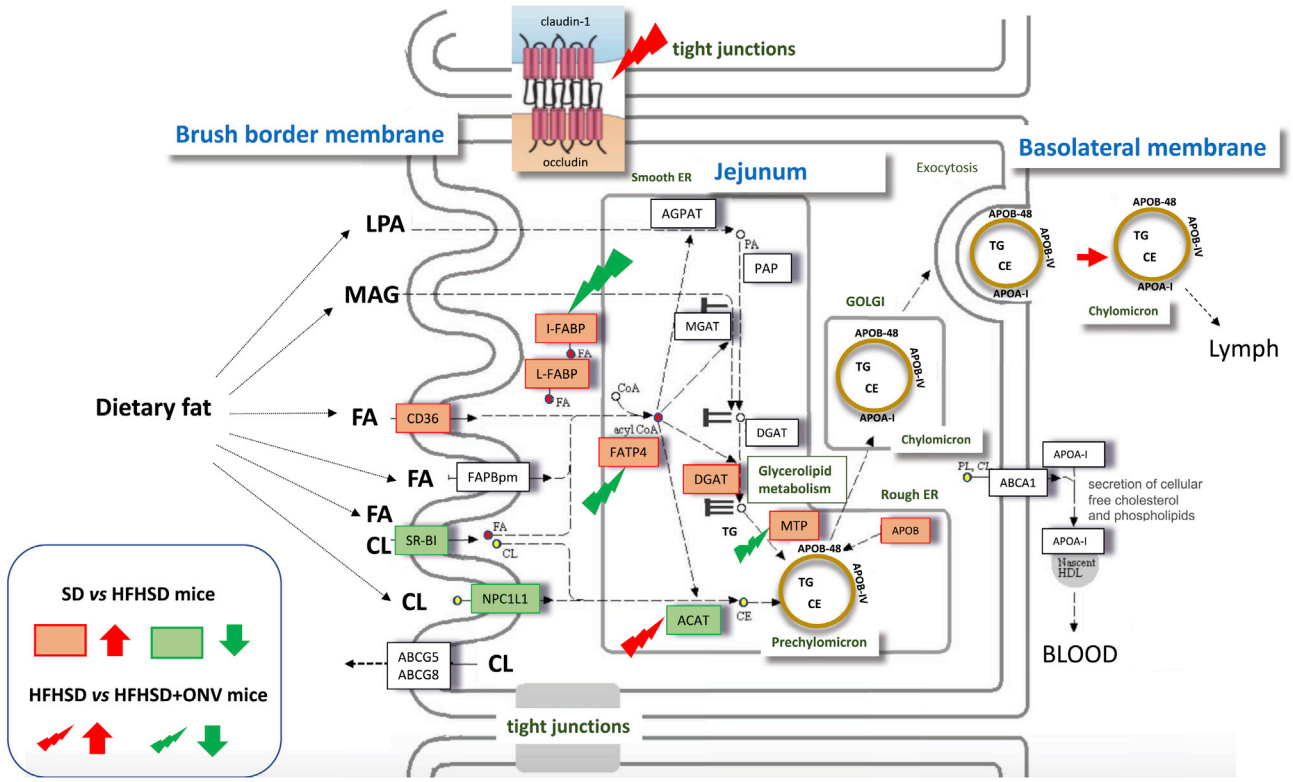

Figure 5. ONVs Regulated Genes Involved in Fat Absorption and Release or Expressed in Tight Junctions in Jejunum

Genes in red, upregulated by the HFHSD versus SD; genes in green, downregulated by the HFHSD versus SD. Red arrows indicate upregulated in HFHSD+ONV mice versus HFHSD mice; green arrows indicate downregulated in HFHSD+ONV mice versus HFHSD mice. SD, n = 5; HFHSD, n = 10; HFHSD+ONV, n = 10.

steatosis (Figures 6D and 6E). Interestingly, blood TG levels were negatively correlated with gastrocnemius weight of HFHSD+ONV mice ($R^2 = -0.56$, $p = 0.046$, Kendall correlations). Collectively, these data suggest that consumption of ONVs could protect the liver from diet-induced lipid storage by reducing the fat absorption by intestine and consequently by the liver and by increasing TG release from the liver, which could be stored in and used by skeletal muscle. The explanations of MTP opposite regulations respectively in intestine and liver deserve further experiments.

DISCUSSION

The small intestinal epithelium is highly responsive to changes in nutrient intake or exposure to luminal nutrients. High intake of carbohydrate and fat have been associated with damage to intestinal mucosa and consequently to a decrease in the function of the IBs. Indeed, induction of intestinal permeability leading to the passage of gut bacteria and to a decrease in the number of immune cells that protect the mucosa have been observed in obese subjects.[29,34] Conversely to what is observed for highly inflammatory pathologies (i.e., acute colitis or Crohn's disease), chronic consumption of a high-fat diet turns off the immune response of the small intestine.[30] In our study, 16 weeks of an HFHSD induced the signs and symptoms of human metabolic syndrome in mice (i.e., obesity, insulin resistance, non-alcoholic fatty liver disease, dyslipidemia, and high plasma TG levels). Transcriptomic analyses in the jejunum confirmed that an HFHSD induced deficiency within the intestinal immune system and modulated genes involved in intestinal permeability. HFHSD mice also had higher dietary fat absorption and increased secretion of chylomicrons.

Six hours post-gavage, ONVs accumulated preferentially in the jejunum. Conversely to what was published for ginger-derived nanovesicles,[11] we did not detect ONVs in liver, suggesting that ONV main localization and first action occurred in the intestinal mucosa. The same intestinal biodistribution was described for grapefruit-derived nanovesicles also from the Rutaceae family.[27] Therefore, associated with their enriched lipid content and specific lipid composition,[35] ONVs accumulated preferentially in the intestinal region involved in dietary lipid absorption. In this region, ONVs induced an increase in villi size, modulated mRNA levels of genes involved in immune response, and decreased jejunum TG content at the fasted state. *In vitro* data with IBs indicated that ONVs were internalized by enterocytes.

Their actions on the jejunum observed in this study could result both from their incorporation into jejunum cells and from their

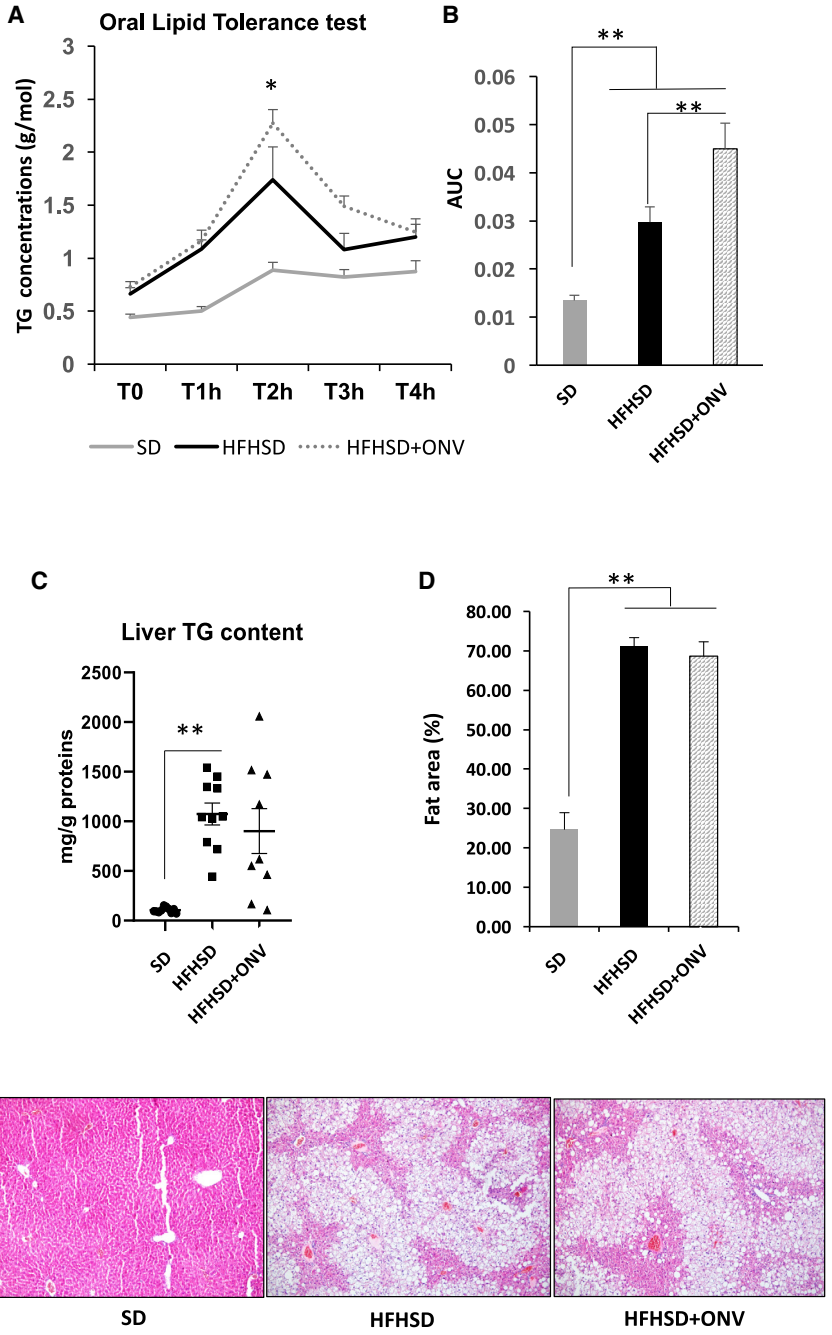

Figure 6. TG Content in Liver and Blood from HFHSD+ONV Mice

(A) Kinetics of plasma TG concentrations after lipid overload (n = 10). (B) Areas under the curves calculated from plasma TG concentrations in (A). (C) Liver TG concentrations at sacrifice (SD, n = 5; HFHSD, n = 10; HFHSD+ONV, n = 10). (D) Hepatic lipid accumulation evaluation by color separation on ImageJ (original magnification, ×100 in three to five fields randomly chosen; n = 5 mice). (E) Representative images used to quantify liver lipid accumulation in (D) (hematoxylin and eosin staining). *p < 0.05, student t test.

composition. In this study we found that ONVs are rapidly incorporated into IBs *in vitro*, which confirms previous studies showing that fruit-derived nanovesicles can be captured by the cells from intestine (e.g., intestinal dendritic cells for broccoli nanovesicles,[13] macrophages for grapefruit nanovesicles,[27] Lgr5^{+} stem cells for grape nanovesicles[10]) and similarly could induce cell growth (i.e., *in vitro* on Caco-2 cells and *in vivo* in jejunum). ONVs contain PA, which controls membrane fission and fusion,[36] and their action on the mTOR pathway could explain part of the actions of ONVs on villi growth in HFHSD mice.[37] In addition, ONVs are enriched in phospholipids, which have important functions for the IB. It is known that obesity is associated with a decrease in mucus thickness.[29] It was demonstrated that PC, *sn*-glycero-3 phosphocholine (POPC), and, to a less extent, PE[38,39] contained in ONVs are essential components of mucus and have anti-inflammatory properties[40] (e.g., patients with ulcerative colitis showed significant restoration of the mucosal barrier after a treatment with PC.[41] Therefore, amelioration of intestinal functions induced by ONVs in HFHSD mouse jejunum might be related to PC and POPC from OVNs.

Compared to previous studies on severe IB alterations showing that edible plant nanovesicles can restore villi size and functions,[10,13,27] obesity-induced intestinal alterations are modest. It is thus interesting to observe that ONVs have an action on a poorly altered barrier even for a limited period of time, meaning that vegetable-derived nanovesicles participate in the maintenance of the IB integrity also in healthy subjects and thus should be preserved during industrial production of fruit juices. In addition to bioactive lipids, their enrichment in leucine compared to juice is physiologically relevant. Indeed, it was demonstrated that increased dietary leucine intake improves glucose metabolism in obese subjects.[42] Indeed, leucine belongs to the category of branched amino acids, and previous studies highlight a reduction of leucine concentration in blood circulation of insulin-resistant patients,[43] which could lead to a lack of leucine distribution in organs required for functioning well. Metabolomic results obtained in the present study on ONVs suggest for the first time that ONVs can cause a local leucine supplementation in the jejunum of obese mice.

Finally, previous studies have also identified small RNAs in fruit-derived nanovesicles. In that context, 113 conserved miRNAs were

identified from ONVs.[44] The authors of this study predicted possible target genes of ONV-derived miRNAs in the mammalian genome, by bioinformatics. They found that one of them, MIR-398b, was predicted to bind IL-1, alpha gene, involved in the immune response. However, beside these predictions, no study so far has firmly demonstrated the functionality of plant-derived miRNA on the mammalian genome and it is still a matter of debate.[45]

In the intestinal lumen, dietary TGs are modified into monoacylglycerol and fatty acids, which are incorporated into micelles and taken up by enterocytes. Once in the enterocytes, monoacylglycerol and fatty acids are re-esterified into TGs and packaged into chylomicrons for secretion. In the context of obesity, the effects of OVNs on villi size in jejunum and thus on the surface of nutrient absorption could have amplified the HFHSD deleterious effects on weight gain and metabolic deterioration. However, analyses of mRNA levels of genes involved in lipid metabolism in enterocytes showed that ONV treatment suppressed the increased FATP4 and FABP2 in the intestine of HFHSD mice. FATP4 is the major intestinal transporter required for efficient uptake of fatty acids,[46] and FABP2 is involved in the intracellular transport of long-chain fatty acid and in TG-rich lipoprotein synthesis. Thus, the data indicated that ONVs decreased fatty acid absorption by the jejunum. ONVs also downregulated mRNA coding for MTP, which has a major role in chylomicron synthesis.[47] This protein is essential for the biosynthesis of TG-rich lipoproteins. MTP also modulates cholesterol ester synthesis by an unknown mechanism.[47] Taken together, these data are in favor of a reduced chylomicron secretion by the jejunum after 1 month of gavage with ONVs in HFHSD mice but not associated with lipid accumulation in the intestine. In the context of metabolic syndrome associated with hyperlipidemia, previous studies have demonstrated that MTP inhibition could be an effective therapeutic target to lower plasma lipids. In our study, 1-month treatment with ONVs was not sufficient to lower blood TG concentration in our model of highly metabolically perturbed obese mice. Longer treatment should thus be considered. A major side effect of MTP inhibitors is that they also inhibit MTP expression in liver and thus induce fat lipid storage in this tissue.[47] Interestingly, ONV treatment did not aggravate liver steatosis, as MTP mRNA level was increased in liver. Therefore, ONVs seem to protect both the intestine and the liver from fat overload associated with the HFHSD. ONVs also triggered the downregulation of angiopoietin-like protein-4 (ANGPL4) mRNA in the jejunum of HFHSD+ONV versus HFHSD mice, a novel target for therapy in regulating and attenuating colonic inflammation.[48]

In conclusion, this study demonstrated that part of the beneficial effects of orange juice on the metabolism and villi size are reproduced by ONVs. Therefore, in the case of obesity-associated diabetes, ONVs could represent an alternative to the consumption of fruit juice. Used as a dietary supplement for a short period of time, ONVs would accelerate the recovery of intestinal functions during weight loss in obese patients. However, we do not recommend the consumption in chronic, and, more generally speaking, the use of fruit-derived nanovesicles for healthy populations. We can not rule out that the induction of villi growth is not associated with the induction of pathways potentially involved in cancer onset and progression. In addition, we demonstrated also that ONVs, and likely all nanovesicles derived from editable plants, concentrate plant species-specific lipids and metabolites that are captured by the IBs and consequently modulate lipid metabolism at the whole-body level. This has to be taken into account in studies using plant-derived nanovesicles for drug delivery,[15] as it might interfere or potentialize drug actions.

MATERIALS AND METHODS

Preparation of ONVs

Untreated oranges (*Citrus sinensis* (L.) Osbeck var. Valencia) were cut into two parts and seeds were removed. The two parts were placed on a juicer, and pressure and twist were applied to extract juice. Juice was centrifuged at 3,000 × *g* (30 min, 4°C) and the supernatant was further centrifuged at 10,000 × *g* (60 min, 4°C) to remove cell debris, fibers, various aggregates and intracellular organelles. After filtration at 100 μm and then at 0.45 μm, juice was centrifuged at 16,500 × *g* (60 min, 4°C) and the supernatant was ultracentrifuged (90 min, 100,000 × *g*, 4°C) (Beckman Coulter, Optima L-80 XP ultracentrifuge, type 50-2Ti rotor). The pellet was rinsed in phosphate-buffered saline (PBS) and resuspended in PBS after ultracentrifugation (90 min, 100,000 × *g*, 4°C). The same procedure was used to extract ONVs from industrial juice with pulp purchased at 4°C, or from industrial juice reconstituted from concentrate, purchased at room temperature. Size exclusion columns (qEV10, Izon Science, France) were used to further purify the ONV pellet.

Imaging of ONV with TEM

ONVs in PBS were adsorbed on 200-mesh nickel grids coated with Formvar-C. After washing once in filtrated distilled water, suspensions were colored with 2% phosphotungstic acid for 2 min and examined using a JEM-1400 transmission electron microscope (JEOL, Tokyo, Japan) equipped with an Orius 600 camera.

Particle Size and Surface Charge Analysis

NanoSight NS300 (Malvern Panalytical, Orsay, France) was used to measure the size of particles.[49] The number of particles and their movement were recorded for 5 × 60 s (camera level = 16). Particle sizes were quantified by nanotracking analysis (NTA, detection threshold = 4) using the NS500 software. The zeta potential was measured with Zetasizer Nano S90.

IB Cell Culture

Caco-2 cells (human colorectal carcinoma cells [ATCC HTB-37], which express characteristics of enterocytic differentiation at confluence) and HT29-MTX cells (human colon carcinoma-derived mucin-secreting goblet cell line) were grown in Dulbecco's modified Eagle's medium (DMEM) with high glucose (4.5 g/L) containing 10% fetal bovine serum (FBS) (DMEM with 10% FBS, PAA Laboratories, Les Mureaux, France) and antibiotics (100 μg/mL streptomycin and 100 U/mL penicillin, Sigma-Aldrich, St. Quentin Fallavier, France). Caco-2 and HT29-MTX cells were grown in co-cultures on inserts (ratio of Caco-2/HT29-MTX = 9:1). 18 days post-confluence,

co-cultures were treated with 10 μM oleic acid for 4 h (Sigma-Aldrich) in serum-free DMEM. We have shown that this treatment induced phenotype reprogramming of Caco-2 cells (reduced proliferation rate and modification of lipid metabolism) and differentiation of HT29-MTX cells (i.e., expression markers of goblet cells and mucus), thus producing an artificial IBs closed to *in vivo* conditions.[50]

Co-culture of IBs with Differentiated Adipocytes to Monitor Adipocyte Lipid Uptake

IBs were grown as described above in 96-well inserts. IBs were treated for 3 h with ONVs. Then, the media were refreshed before loading IB-containing inserts onto E-plates containing 3T3-L1 MXB adipocytes already differentiated, as previously described[28] (ATCC CRL-3242, Sigma-Aldrich). Variations of cell impedance of 3T3-L1 MXB adipocytes were monitored in real time for 22 h using the xCELLigence system (every 5 min during 50 cycles, then every 15 min until 22 h). As differentiated 3T3-L1 MXB adipocytes are proliferative, any modification of cell impedance is associated with variation of their morphologies, and thus lipid uptake or lipolysis was used as described and validated previously.[28,51] Data are represented as the cell index normalized to time (T) = 0 (delta cell index ± SEM), where the cell index = slope × time + intercept. At the end of the experiments, IB cells and adipocytes were trypsinized for analysis with flow cytometry. For quantification of TGs and ROS on fixed cells, IBs were fixed with 3% formalin (Sigma-Aldrich) then incubated with an AdipoRed assay (TG quantifications), washed in PBS, and treated with 2.5 μg/mL dihydrorhodamine-6G (DHR6G) (#C262, tebu-bio) in PBS with 0.1% Triton X-100 (ROS quantification). Nuclei were labeled with Hoechst 33258. Fluorescence intensities were measured by using the Cytation 3 platform (BioTek Instruments, Colmar, France) at 350 nm (excitation)/461 nm (emission) for Hoechst 33258, at 535 nm/572 nm for AdipoRed, and at 528 nm/551 nm for DHR6G (objective ×4). Lipid droplet number and size in adipocytes and cell number were determined by measuring fluorescence intensities from images recorded and analyzed using Cytation 3 (magnification ×4)

ONV Uptake by Caco-2 Cells and IBs

To detect ONV incorporation in intestinal cells, ONVs were labeled with PKH67, according to the manufacturer's protocol. ONVs were resuspended in 250 μL of diluent C. Separately, 250 μL of diluent C was mixed with 2 μL of PKH67 to prepare the staining solution. The resuspended ONVs were mixed with the PKH67 solution and incubated for 5 min. The labeling reaction was stopped with one equal volume of 1% BSA. Labeled ONVs were purified and used to treat IBs. After 24 h, IBs were trypsinized and fluorescent cells were counted by flow cytometry. Labeled ONVs were also used to treat monocultures of Caco-2 cells for 6 h in the presence of endocytosis inhibitors (1 μM cytochalasin D together with ONVs, and 100 μM indomethacin 30 min before adding ONVs) (Sigma-Aldrich). After washing in PBS, cells were counterstained with Hoechst 3342 and fixed in 3.7% formaldehyde solution for 5 min at room temperature (RT) and blocked with 5% BSA in PBS. Fluorescence intensities were quantified with the Cytation 3 cell imaging reader (BioTek Instruments, Colmar, France).

Lipidomic Analyses

Glycerolipids were extracted from 1 mg equivalent protein freeze-dried ONV pellets by addition of 2 mL of methanol and 8 mL of chloroform at room temperature. The mixture was then saturated with argon and stirred for 1 h at room temperature. 3 mL of chloroform/methanol (2:1 ratio) and 5 mL of 1% NaCl were then added to solution to initiate biphase formation. The chloroform phase was dried under argon before solubilizing the lipid extract in pure chloroform. Lipid extracts were dissolved in 100 μL of chloroform/methanol (2:1 ratio) containing 125 pmol of each internal standard.[52] The lipid classes were separated using an Agilent 1200 high-performance liquid chromatography (HPLC) system using a 150 × 3-mm (length × internal diameter) 5-μm diol column (Macherey-Nagel) at 40°C.[52] The distinct glycerophospholipid classes were eluted successively as a function of the polar head group in the following order: triacylglycerol (TAG), DAG, monogalactosyldiacylglycerol (MGDG), digalactosyldiacylglycerol (DGDG), phosphatidylethanolamine (PE), 1,2-dipalmitoyl-*sn*-glycero-3-*O*-4'-(*N*,*N*,*N*-trimethyl)-homoserine (DGTS), diacylglycerylhydroxymethyl-*N*,*N*,*N*-trimethyl-β-alanine (DGTA), phosphatidylglycerol (PG), phosphatidylinositol (PI), sulfoquinovosyl diacylglycerol (SQDG), phosphatidylserine (PS), phosphatidylcholine (PC), diphosphatidylglycerol (DPG), and phosphatidic acid (PA). Knowing the mass of each glycerolipid potentially present, lipid extracts were thereafter analyzed by liquid chromatography-tandem mass spectrometry (LC-MS/MS).[53] Lipid amounts (pmol) were corrected for response differences between internal standards and endogenous lipids and by comparison with a qualified control (QC). The QC extract corresponded to a known lipid extract from *Arabidopsis* cell culture qualified and quantified by thin layer chromatography (TLC) and gas chromatography with flame-ionization detection (GC-FID).[53]

Metabolomic Analyses by NMR

540 μL of PBS containing ONVs extracted from 165 mL of pure orange juice or 540 μL of pure orange juice were mixed with 60 μL of phosphate buffer (pH 7.4) (160 mM Na_2HPO_4, 30 mM NaH_2PO_4, 1 mM trimethylsilylpropanoate (TSP), and 3 mM NaN_3 in 100% deuterium oxide [D_2O]) and transferred to 5 mm NMR tubes.[54] All NMR experiments were acquired on a 600-MHz Bruker NMR spectrometer with a 5-mm TCI CryoProbe (Bruker BioSpin, Rheinstetten, Germany). Temperature was fixed at 30.0°C throughout the experiments. For each sample, two types of 1D experiments were recorded, using a standard pulse sequence: Carr-Purcell-Meiboom-Gill (CPMG, cpmgpr1d) (Meiboom and Gill, 1958) and 1D Nuclear Overhauser Effect Spectroscopy (NOESY) (noesypr1d, mixing time 10 ms), both with water suppression applied during the relaxation time for 4 s, 128 transient free induction decays (FIDs), and a spectral width of 20 ppm[55]. All FIDs were multiplied by an exponential function corresponding to a 0.3-Hz line-broadening factor prior to Fourier transform and ^{1}H-NMR spectra were manually phased and referenced to the glucose doublet at 5.23 ppm using TopSpin 4.0. Identification of the metabolites was carried out from the 1D NMR spectra using the software Chenomx NMR Suite 8.0 (Chenomx, Edmonton, AB, Canada) and confirmed from analysis of 2D ^{1}H-^{1}H

Total Correlation Spectroscopy (TOCSY), ^{1}H-^{13}C Heteronuclear single quantum coherence (HSQC) spectroscopy, and ^{1}H J-resolved NMR spectra recorded with standard parameters. The measured multiplet chemical shifts were compared to reference shifts of pure compounds using the HMDB database.[56] A pure standard lactate solution (1 g/L, Fisher Scientific) was used as an external concentration reference and exploited using the ERETIC2 utility from TopSpin (Bruker, Rheinstetten, Germany) to add a digitally synthesized peak to a spectrum as recommended in Jung et al.[57] Lactate-relative metabolite concentrations were determined using Chenomx software by manual fitting of the proton resonance lines for the compounds available in the database. The linewidth was adjusted to the width of one component of the alanine doublet.

ONV In Vivo *Biodistribution*

ONVs were pelled in the presence of 1 μM fluorescent lipophilic tracer DiR (1,1-dioctadecyl-3,3,3,3-tetramethylindotricarbocyanine iodide) (D12731, Invitrogen) by ultracentrifugation (110,000 × *g*, 90 min). Mice received either 150 μg of DIR-labeled ONVs[58] or mock-PBS-DiR as control through gavage. Six hours after gavage, animals were sacrificed and the organs were carefully harvested and imaged for 2 s (excitation, 710 nm; emission, 760 nm) using a high sensitivity charge-coupled device (CCD) camera *in vivo* imaging system (IVIS) Spectrum (PerkinElmer, USA). Data were normalized on mock-PBS-DiR. Experiments were approved by the Swedish Local Board for laboratory animals and were performed in accordance with ethics permission and designed to minimize animal suffering and pain.

Protocol with Diet-Induced Obese (DIO) Mice

4-week-old male mice were purchased from Envigo. Animals (n = 30) were housed in the common animal center from the AniRA-PBES core facility (ENS Lyon, France) at 22°C and with a 12-h light/12-h dark cycle. Animal procedures were conducted in accordance with the French institutional guidelines for the care and use of laboratory animals (ethic committee number: APAFIS#10279-2017041216448928). After 1 week of acclimatization, mice were divided into two groups: one was given free access to a standard chow diet (n = 10 SD, Rhod-16A, Genobios) and another one was given free access to a pelleted HFHSD (n = 20 HFHSD, 36% fat, 35% carbohydrate [50% sucrose], and 19.8% protein; TD99249; Harlan Laboratories). After 12 weeks, a GTT (1 mg of glucose/g body weight) and ITT (0.75 mU of insulin/body weight) were performed to confirm that HFHSD mice were glucose-intolerant, insulin-resistant, and hyperinsulinemic in addition to being obese.[59] Then, HFHSD animals were divided into two groups, both continuing the HFHS diet: one receiving 100 μL of PBS (n = 10, HFHSD) and one receiving 150 μg of ONVs in 100 μL of PBS through gavage (5 days/week, 4 weeks) (n = 10, HFHSD+ONV). Considering that a human of 80 kg can drink 1 mg of ONVs per 350 mL of fresh orange juice per day, obese diabetic mice of 45 g would consume 560 μg of ONVs. However, based on previous publications on juice-derived vesicles (Table S1 in Rome[1]), and on our *in vitro* data showing a toxicity of ONVs at high concentrations, we have preferred to decrease the concentration to 150 μg for the gavage. Of note, ONV pellets were rinsed three times in PBS to remove acidity of the solution before gavage. At 15 weeks, n = 5 animals per group received 200 μL of commercial vegetable oil (Lesieur Isio 4, France) at the 6-h fasted state and blood was withdrawn from the tail every hour for 4 h. TGs were quantified in plasma at each time point. At 15 weeks, GTTs and ITTs were again performed to determine the impact of ONVs on metabolic parameters. At 12 and 16 weeks, plasma glucose levels were determined at the fasted state by using the Accu-Chek Performa glucometer (Roche Diabetes Care France, Meylan, France). At 16 weeks, fasting plasma insulin was determined with mouse ultrasensitive ELISA (Eurobio, Courtaboeuf, France). Then, animals were sacrificed and the gastrointestinal tract, skeletal muscles, liver, and adipose tissues were rapidly removed and frozen in liquid nitrogen or fixed for further analyses.

Histology Analyses

Liver and gut biopsies were fixed in 4% formaldehyde/phosphate buffer for 24 h at 4°C, then dehydrated and embedded in paraffin. 5-μm-thick sections were stained with hematoxylin and eosin. The percentage of macrovesicular steatosis in liver sections was assessed by lipid droplet detection and segmentation at ×100 magnification in three to five fields per randomly chosen image.[60,61]

Statistical Analyses

Unpaired two-tailed Student's t tests and analyses of variance (ANOVAs) with corresponding *post hoc* tests were performed using GraphPad Prism (GraphPad, La Jolla, CA, USA). The one-way ANOVA test for independent measures was used to compare the means of three independent samples simultaneously. Correlations analyses were performed using R (v3.5) using a non-parametric approach (Kendall rank correlation coefficient). Data are expressed as mean ± SEM. The cutoff for significance level was set at $p \leq 0.05$.

SUPPLEMENTAL INFORMATION

Supplemental Information can be found online at https://doi.org/10.1016/j.omtm.2020.08.009.

AUTHOR CONTRIBUTIONS

E.B.: conceived and performed all *in vitro* data, wrote the paper, and corrected all figures; P.C.: ONV extraction for ONV characterization and lipid analyses and for *in vivo* experiments, corrected part of the Materials and Methods section; A.J.: ONV extraction for metabolic analyses and *in vivo* experiments, TG quantification in tissues and blood, RNA extractions in tissues and qRT-PCR analyses, critical analyses of the results; E.M.: statistical analyses with R package and critical reading of the manuscript; O.P.B.W., D.G. and S.E.-A.: ONV biodistribution in mice, manuscript corrections and critical reading; J.J.: lipidomic analyses; E.E.-C.: transmission electron microscopy; S.C.: histology in jejunum and liver; G.J.P.R. and B.P.: metabolomic analyses and critical reading of the manuscript; A.G.: constructive discussions and critical reading of the manuscript; J.R.: all protocols with mice (design and realization), gavage, with ONVs, analyses of metabolic data, and critical reading of the manuscript; S.R.: conceived the study, designed and coordinated the experiments, analyzed all data, and wrote the paper.

CONFLICTS OF DIFFERENCE

The authors declare no competing interests.

ACKNOWLEDGMENTS

We thank Aymeric Audfray and Cédric Brossard from Malvern Panalytical SAS, Venissieux, France, for ONV characterization with NTA NS300 and Zetasizer. This work was supported by the Olga Tribalat Institute (France), the Benjamin Delessert Institute (France), and by INRAe (France). Financial support from the INFRASTRUCTURES DE RECHERCHE Résonance Magnétique Nucléaire, Très Hauts Champs Fr3050 CNRS (France) for conducting the research is also gratefully acknowledged.

REFERENCES

1. Rome, S. (2019). Biological properties of plant-derived extracellular vesicles. Food Funct. *10*, 529–538.
2. An, Q., Hückelhoven, R., Kogel, K.H., and van Bel, A.J. (2006). Multivesicular bodies participate in a cell wall-associated defence response in barley leaves attacked by the pathogenic powdery mildew fungus. Cell. Microbiol. *8*, 1009–1019.
3. An, Q., van Bel, A.J., and Hückelhoven, R. (2007). Do plant cells secrete exosomes derived from multivesicular bodies? Plant Signal. Behav. *2*, 4–7.
4. Cai, Q., Qiao, L., Wang, M., He, B., Lin, F.M., Palmquist, J., Huang, S.D., and Jin, H. (2018). Plants send small RNAs in extracellular vesicles to fungal pathogen to silence virulence genes. Science *360*, 1126–1129.
5. Rutter, B.D., and Innes, R.W. (2017). Extracellular vesicles isolated from the leaf apoplast carry stress-response proteins. Plant Physiol. *173*, 728–741.
6. Rutter, B.D., and Innes, R.W. (2018). Extracellular vesicles as key mediators of plant-microbe interactions. Curr. Opin. Plant Biol. *44*, 16–22.
7. Zhang, M., Viennois, E., Prasad, M., Zhang, Y., Wang, L., Zhang, Z., Han, M.K., Xiao, B., Xu, C., Srinivasan, S., and Merlin, D. (2016). Edible ginger-derived nanoparticles: a novel therapeutic approach for the prevention and treatment of inflammatory bowel disease and colitis-associated cancer. Biomaterials *101*, 321–340.
8. Zhang, M., Viennois, E., Xu, C., and Merlin, D. (2016). Plant derived edible nanoparticles as a new therapeutic approach against diseases. Tissue Barriers *4*, e1134415.
9. Raimondo, S., Naselli, F., Fontana, S., Monteleone, F., Lo Dico, A., Saieva, L., Zito, G., Flugy, A., Manno, M., Di Bella, M.A., et al. (2015). Citrus limon-derived nanovesicles inhibit cancer cell proliferation and suppress CML xenograft growth by inducing TRAIL-mediated cell death. Oncotarget *6*, 19514–19527.
10. Ju, S., Mu, J., Dokland, T., Zhuang, X., Wang, Q., Jiang, H., Xiang, X., Deng, Z.B., Wang, B., Zhang, L., et al. (2013). Grape exosome-like nanoparticles induce intestinal stem cells and protect mice from DSS-induced colitis. Mol. Ther. *21*, 1345–1357.
11. Zhuang, X., Deng, Z.B., Mu, J., Zhang, L., Yan, J., Miller, D., Feng, W., McClain, C.J., and Zhang, H.G. (2015). Ginger-derived nanoparticles protect against alcohol-induced liver damage. J. Extracell. Vesicles *4*, 28713.
12. Zhang, M., Wang, X., Han, M.K., Collins, J.F., and Merlin, D. (2017). Oral administration of ginger-derived nanolipids loaded with siRNA as a novel approach for efficient siRNA drug delivery to treat ulcerative colitis. Nanomedicine (Lond.) *12*, 1927–1943.
13. Deng, Z., Rong, Y., Teng, Y., Mu, J., Zhuang, X., Tseng, M., Samykutty, A., Zhang, L., Yan, J., Miller, D., et al. (2017). Broccoli-derived nanoparticle inhibits mouse colitis by activating dendritic cell AMP-activated protein kinase. Mol. Ther. *25*, 1641–1654.
14. Teng, Y., Ren, Y., Sayed, M., Hu, X., Lei, C., Kumar, A., Hutchins, E., Mu, J., Deng, Z., Luo, C., et al. (2018). Plant-derived exosomal microRNAs shape the gut microbiota. Cell Host Microbe *24*, 637–652.e8.
15. Yang, C., Zhang, M., and Merlin, D. (2018). Advances in plant-derived edible nanoparticle-based lipid nano-drug delivery systems as therapeutic nanomedicines. J. Mater. Chem. B Mater. Biol. Med. *6*, 1312–1321.
16. Salamone, F., Li Volti, G., Titta, L., Puzzo, L., Barbagallo, I., La Delia, F., Zelber-Sagi, S., Malaguarnera, M., Pelicci, P.G., Giorgio, M., and Galvano, F. (2012). Moro orange juice prevents fatty liver in mice. World J. Gastroenterol. *18*, 3862–3868.
17. Simpson, E.J., Mendis, B., and Macdonald, I.A. (2016). Orange juice consumption and its effect on blood lipid profile and indices of the metabolic syndrome; a randomised, controlled trial in an at-risk population. Food Funct. *7*, 1884–1891.
18. Escudero-López, B., Berná, G., Ortega, Á., Herrero-Martín, G., Cerrillo, I., Martín, F., and Fernández-Pachón, M.S. (2015). Consumption of orange fermented beverage reduces cardiovascular risk factors in healthy mice. Food Chem. Toxicol. *78*, 78–85.
19. Morand, C., Dubray, C., Milenkovic, D., Lioger, D., Martin, J.F., Scalbert, A., and Mazur, A. (2011). Hesperidin contributes to the vascular protective effects of orange juice: a randomized crossover study in healthy volunteers. Am. J. Clin. Nutr. *93*, 73–80.
20. Miyagi, Y., Om, A.S., Chee, K.M., and Bennink, M.R. (2000). Inhibition of azoxymethane-induced colon cancer by orange juice. Nutr. Cancer *36*, 224–229.
21. Ribeiro, C., Dourado, G., and Cesar, T. (2017). Orange juice allied to a reduced-calorie diet results in weight loss and ameliorates obesity-related biomarkers: a randomized controlled trial. Nutrition *38*, 13–19.
22. Khan, R.A., Mallick, N., and Feroz, Z. (2016). Anti-inflammatory effects of *Citrus sinensis* L., *Citrus paradisi* L. and their combinations. Pak. J. Pharm. Sci. *29*, 843–852.
23. Deopurkar, R., Ghanim, H., Friedman, J., Abuaysheh, S., Sia, C.L., Mohanty, P., Viswanathan, P., Chaudhuri, A., and Dandona, P. (2010). Differential effects of cream, glucose, and orange juice on inflammation, endotoxin, and the expression of Toll-like receptor-4 and suppressor of cytokine signaling-3. Diabetes Care *33*, 991–997.
24. Rocha, D.M.U.P., Lopes, L.L., da Silva, A., Oliveira, L.L., Bressan, J., and Hermsdorff, H.H.M. (2017). Orange juice modulates proinflammatory cytokines after high-fat saturated meal consumption. Food Funct. *8*, 4396–4403.
25. Randolp, A.B.K., Bhambra, A., Boarder, M., Budriesi, R., Zhong, C., Micucci, M., Ruparelia, K., Surichan, S., and Androutsopoulos, V. (2014). Phytoestrogens as natural prodrugs in cancer prevention: towards a mechanistic model. Phytochem. Rev. *13*, 853–866.
26. Hosseinpour, M., Ehteram, H., Farhadi, M., and Behdad, S. (2012). Evaluation of dextrose water, black tea and orange juice on histopathologic recovery of surgery-induced intestinal damage in rabbits. Trauma Mon. *17*, 275–278.
27. Wang, B., Zhuang, X., Deng, Z.B., Jiang, H., Mu, J., Wang, Q., Xiang, X., Guo, H., Zhang, L., Dryden, G., et al. (2014). Targeted drug delivery to intestinal macrophages by bioactive nanovesicles released from grapefruit. Mol. Ther. *22*, 522–534.
28. Berger, E., and Géloën, A. (2019). Adipocytes as lipid sensors of oleic acid transport through a functional Caco-2/HT29-MTX intestinal barrier. Adipocyte *8*, 83–97.
29. Rohr, M.W., Narasimhulu, C.A., Rudeski-Rohr, T.A., and Parthasarathy, S. (2020). Negative effects of a high-fat diet on intestinal permeability: a review. Adv. Nutr. *11*, 77–91.
30. Johnson, A.M., Costanzo, A., Gareau, M.G., Armando, A.M., Quehenberger, O., Jameson, J.M., and Olefsky, J.M. (2015). High fat diet causes depletion of intestinal eosinophils associated with intestinal permeability. PLoS ONE *10*, e0122195.
31. Lu, P., Sodhi, C.P., and Hackam, D.J. (2014). Toll-like receptor regulation of intestinal development and inflammation in the pathogenesis of necrotizing enterocolitis. Pathophysiology *21*, 81–93.
32. Riehl, T.E., Foster, L., and Stenson, W.F. (2012). Hyaluronic acid is radioprotective in the intestine through a TLR4 and COX-2-mediated mechanism. Am. J. Physiol. Gastrointest. Liver Physiol. *302*, G309–G316.
33. Mattijssen, F., Alex, S., Swarts, H.J., Groen, A.K., van Schothorst, E.M., and Kersten, S. (2013). Angptl4 serves as an endogenous inhibitor of intestinal lipid digestion. Mol. Metab. *3*, 135–144.
34. Bischoff, S.C., Barbara, G., Buurman, W., Ockhuizen, T., Schulzke, J.D., Serino, M., Tilg, H., Watson, A., and Wells, J.M. (2014). Intestinal permeability—a new target for disease prevention and therapy. BMC Gastroenterol. *14*, 189.
35. Ikeda, I., Imaizumi, K., and Sugano, M. (1987). Absorption and transport of base moieties of phosphatidylcholine and phosphatidylethanolamine in rats. Biochim. Biophys. Acta *921*, 245–253.

36. Wang, X., Devaiah, S.P., Zhang, W., and Welti, R. (2006). Signaling functions of phosphatidic acid. Prog. Lipid Res. *45*, 250–278.

37. Fang, Y., Vilella-Bach, M., Bachmann, R., Flanigan, A., and Chen, J. (2001). Phosphatidic acid-mediated mitogenic activation of mTOR signaling. Science *294*, 1942–1945.

38. Braun, A., Treede, I., Gotthardt, D., Tietje, A., Zahn, A., Ruhwald, R., Schoenfeld, U., Welsch, T., Kienle, P., Erben, G., et al. (2009). Alterations of phospholipid concentration and species composition of the intestinal mucus barrier in ulcerative colitis: a clue to pathogenesis. Inflamm. Bowel Dis. *15*, 1705–1720.

39. Le Kim, D., and Betzing, H. (1976). Intestinal absorption of polyunsaturated phosphatidylcholine in the rat. Hoppe Seylers Z. Physiol. Chem. *357*, 1321–1331.

40. Schneider, H., Braun, A., Füllekrug, J., Stremmel, W., and Ehehalt, R. (2010). Lipid based therapy for ulcerative colitis-modulation of intestinal mucus membrane phospholipids as a tool to influence inflammation. Int. J. Mol. Sci. *11*, 4149–4164.

41. Karner, M., Kocjan, A., Stein, J., Schreiber, S., von Boyen, G., Uebel, P., Schmidt, C., Kupcinskas, L., Dina, I., Zuelch, F., et al. (2014). First multicenter study of modified release phosphatidylcholine "LT-02" in ulcerative colitis: a randomized, placebo-controlled trial in mesalazine-refractory courses. Am. J. Gastroenterol. *109*, 1041–1051.

42. Zhang, Y., Guo, K., LeBlanc, R.E., Loh, D., Schwartz, G.J., and Yu, Y.H. (2007). Increasing dietary leucine intake reduces diet-induced obesity and improves glucose and cholesterol metabolism in mice via multimechanisms. Diabetes *56*, 1647–1654.

43. Karusheva, Y., Koessler, T., Strassburger, K., Markgraf, D., Mastrototaro, L., Jelenik, T., Simon, M.C., Pesta, D., Zaharia, O.P., Bódis, K., et al. (2019). Short-term dietary reduction of branched-chain amino acids reduces meal-induced insulin secretion and modifies microbiome composition in type 2 diabetes: a randomized controlled crossover trial. Am. J. Clin. Nutr. *110*, 1098–1107.

44. Xiao, J., Feng, S., Wang, X., Long, K., Luo, Y., Wang, Y., Ma, J., Tang, Q., Jin, L., Li, X., and Li, M. (2018). Identification of exosome-like nanoparticle-derived microRNAs from 11 edible fruits and vegetables. PeerJ *6*, e5186.

45. Wang, W., Liu, D., Zhang, X., Chen, D., Cheng, Y., and Shen, F. (2018). Plant microRNAs in cross-kingdom regulation of gene expression. Int. J. Mol. Sci. *19*, 2007.

46. Stahl, A., Hirsch, D.J., Gimeno, R.E., Punreddy, S., Ge, P., Watson, N., Patel, S., Kotler, M., Raimondi, A., Tartaglia, L.A., and Lodish, H.F. (1999). Identification of the major intestinal fatty acid transport protein. Mol. Cell *4*, 299–308.

47. Hussain, M.M., Rava, P., Walsh, M., Rana, M., and Iqbal, J. (2012). Multiple functions of microsomal triglyceride transfer protein. Nutr. Metab. (Lond.) *9*, 14.

48. Phua, T., Sng, M.K., Tan, E.H., Chee, D.S., Li, Y., Wee, J.W., Teo, Z., Chan, J.S., Lim, M.M., Tan, C.K., et al. (2017). Angiopoietin-like 4 mediates colonic inflammation by regulating chemokine transcript stability via tristetraprolin. Sci. Rep. *7*, 44351.

49. Filipe, V., Hawe, A., and Jiskoot, W. (2010). Critical evaluation of nanoparticle tracking analysis (NTA) by NanoSight for the measurement of nanoparticles and protein aggregates. Pharm. Res. *27*, 796–810.

50. Berger, E., Nassra, M., Atgié, C., Plaisancié, P., and Géloën, A. (2017). Oleic acid uptake reveals the rescued enterocyte phenotype of colon cancer Caco-2 by HT29-MTX cells in co-culture mode. Int. J. Mol. Sci. *18*, 1573.

51. Berger, E., Héraud, S., Mojallal, A., Lequeux, C., Weiss-Gayet, M., Damour, O., and Géloën, A. (2015). Pathways commonly dysregulated in mouse and human obese adipose tissue: FAT/CD36 modulates differentiation and lipogenesis. Adipocyte *4*, 161–180.

52. Jouhet, J., Maréchal, E., Bligny, R., Joyard, J., and Block, M.A. (2003). Transient increase of phosphatidylcholine in plant cells in response to phosphate deprivation. FEBS Lett. *544*, 63–68.

53. Jouhet, J., Lupette, J., Clerc, O., Magneschi, L., Bedhomme, M., Collin, S., Roy, S., Maréchal, E., and Rébeillé, F. (2017). LC-MS/MS versus TLC plus GC methods: consistency of glycerolipid and fatty acid profiles in microalgae and higher plant cells and effect of a nitrogen starvation. PLoS ONE *12*, e0182423.

54. Beckonert, O., Keun, H.C., Ebbels, T.M., Bundy, J., Holmes, E., Lindon, J.C., and Nicholson, J.K. (2007). Metabolic profiling, metabolomic and metabonomic procedures for NMR spectroscopy of urine, plasma, serum and tissue extracts. Nat. Protoc. *2*, 2692–2703.

55. Meiboom, S., and Gill, D. (1958). Modified spin-echo method for measuring nuclear relaxation times. Rev. Sc. Instrum. *29*, 688.

56. Wishart, D.S., Feunang, Y.D., Marcu, A., Guo, A.C., Liang, K., Vázquez-Fresno, R., Sajed, T., Johnson, D., Li, C., Karu, N., et al. (2018). HMDB 4.0: the human metabolome database for 2018. Nucleic Acids Res. *46* (D1), D608–D617.

57. Jung, Y.S., Hyeon, J.S., and Hwang, G.S. (2016). Software-assisted serum metabolite quantification using NMR. Anal. Chim. Acta *934*, 194–202.

58. Wiklander, O.P., Nordin, J.Z., O'Loughlin, A., Gustafsson, Y., Corso, G., Mäger, I., Vader, P., Lee, Y., Sork, H., Seow, Y., et al. (2015). Extracellular vesicle in vivo biodistribution is determined by cell source, route of administration and targeting. J. Extracell. Vesicles *4*, 26316.

59. Bonnard, C., Durand, A., Peyrol, S., Chanseaume, E., Chauvin, M.A., Morio, B., Vidal, H., and Rieusset, J. (2008). Mitochondrial dysfunction results from oxidative stress in the skeletal muscle of diet-induced insulin-resistant mice. J. Clin. Invest. *118*, 789–800.

60. Levene, A.P., Kudo, H., Armstrong, M.J., Thursz, M.R., Gedroyc, W.M., Anstee, Q.M., and Goldin, R.D. (2012). Quantifying hepatic steatosis—more than meets the eye. Histopathology *60*, 971–981.

61. Nativ, N.I., Chen, A.I., Yarmush, G., Henry, S.D., Lefkowitch, J.H., Klein, K.M., Maguire, T.J., Schloss, R., Guarrera, J.V., Berthiaume, F., and Yarmush, M.L. (2014). Automated image analysis method for detecting and quantifying macrovesicular steatosis in hematoxylin and eosin-stained histology images of human livers. Liver Transpl. *20*, 228–236.

OMTM, Volume *18*

Supplemental Information

Use of Nanovesicles from Orange Juice to Reverse Diet-Induced Gut Modifications in Diet-Induced Obese Mice

Emmanuelle Berger, Pascal Colosetti, Audrey Jalabert, Emmanuelle Meugnier, Oscar P.B. Wiklander, Juliette Jouhet, Elisabeth Errazurig-Cerda, Stéphanie Chanon, Dhanu Gupta, Gilles J.P. Rautureau, Alain Geloen, Samir El-Andaloussi, Baptiste Panthu, Jennifer Rieusset, and Sophie Rome

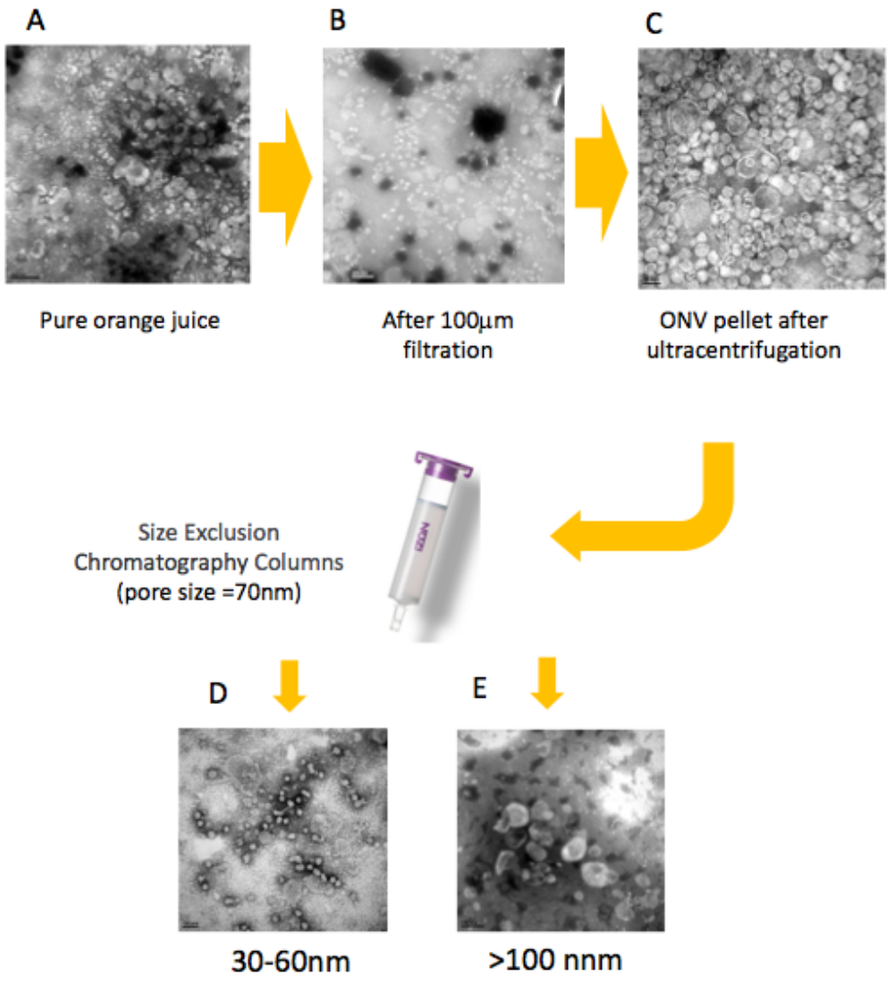

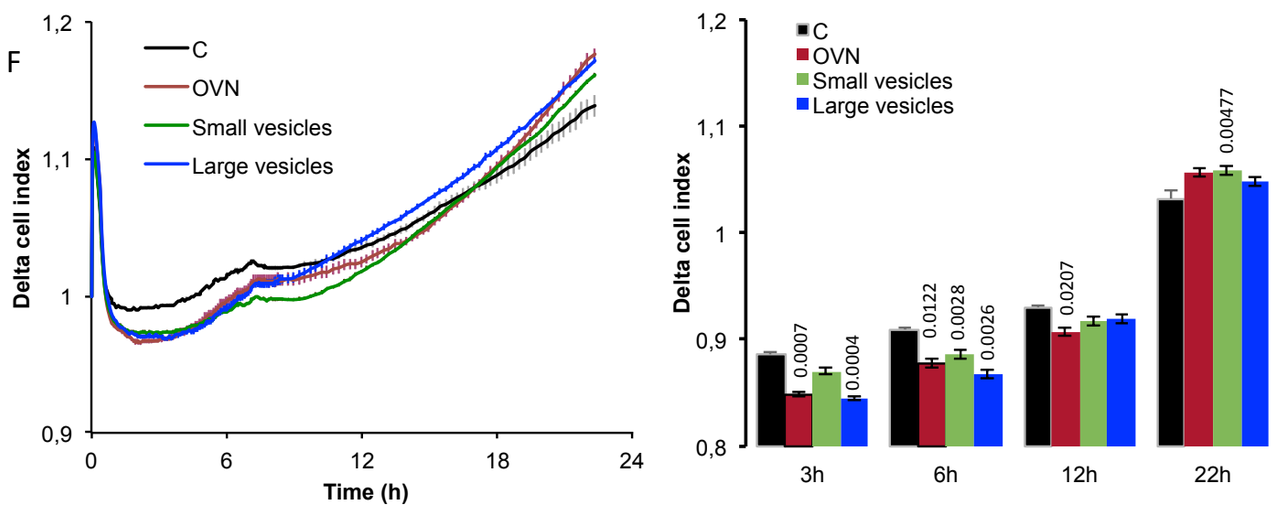

Figure S1: Transmission Electron Microscopy (TEM) images from: (A) pure orange juice; (B) after the first step of orange juice filtration at 100 µm; (C) from the pellet after ultracentrifugation and resuspension in PBS. (Bar=200nm). (D and E) ONV pellet re-suspended in PBS was further passed through a size exclusion column (IZON) and fractions containing proteins were visualized by TEM (Bar=100nm). (F) The activities of the small (D) and large vesicles (E) was tested independently on Caco-2 cells by using the xCELLigence live cell analysis System. Caco-2 cells were plated on 96-wells E-plates at 2500 cells/well in DMEM/10% FBS for 3 days then maintained in DMEM/5% FBS exosome-free for 2 hours before treatment with 2 µg/ml of either small or large vesicles, or ONV. The left panel represents real-time monitoring of the cell index substracted from the cell index at T=0 (mean delta cell index, every 5 min during 50 cycles then every 15 min) for 22 h. The right panel represents the slopes at T=22h (mean values +/- sem) (n=4 to 6 replicates), with significant p-values (*=p<0.05, each condition vs untreated caco-2).

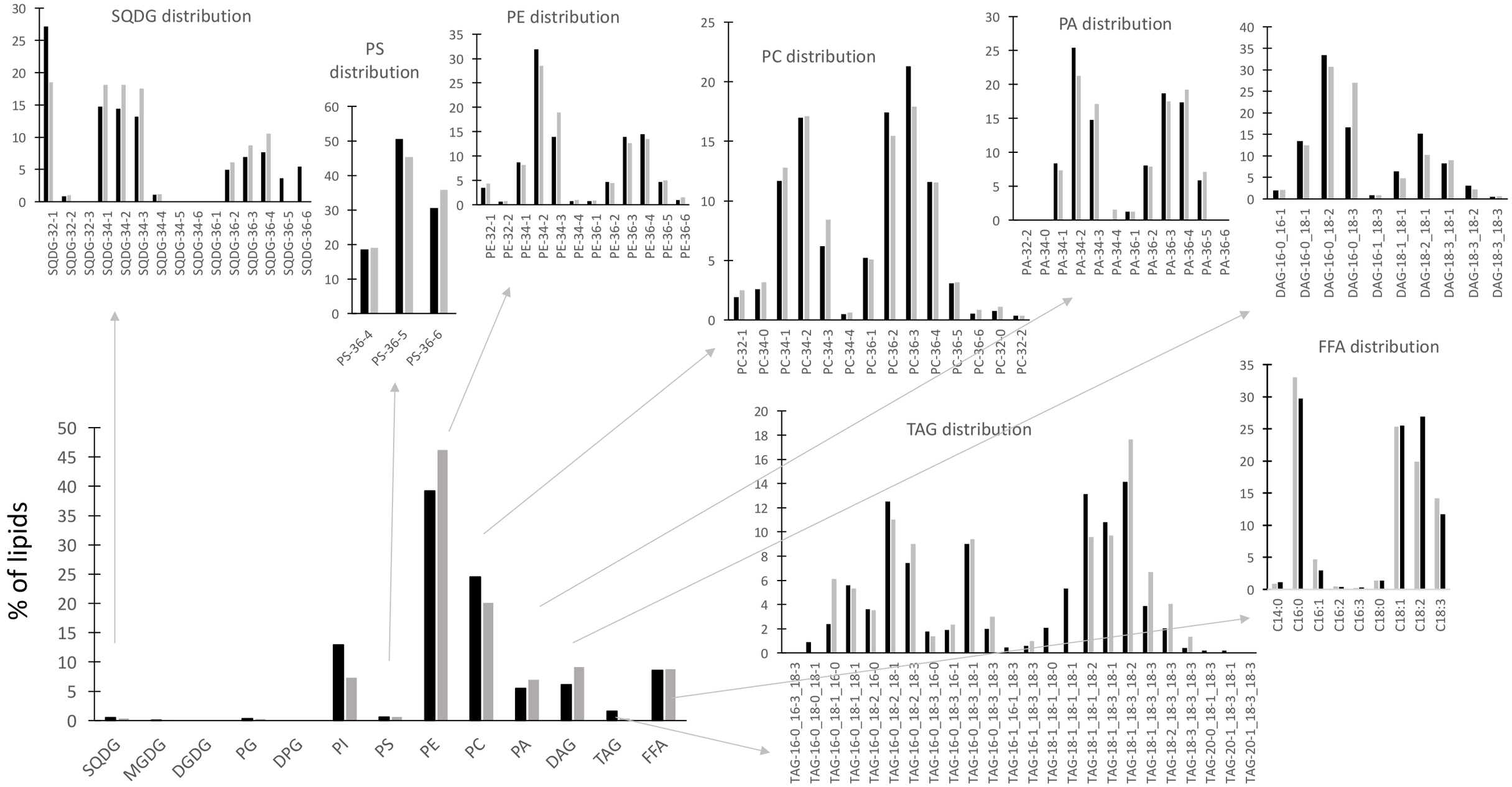

Figure S2: Lipidomic analyses from 1mg ONV. The two colors represent two independent lipidomic analyses from 2 independent ONV preparations

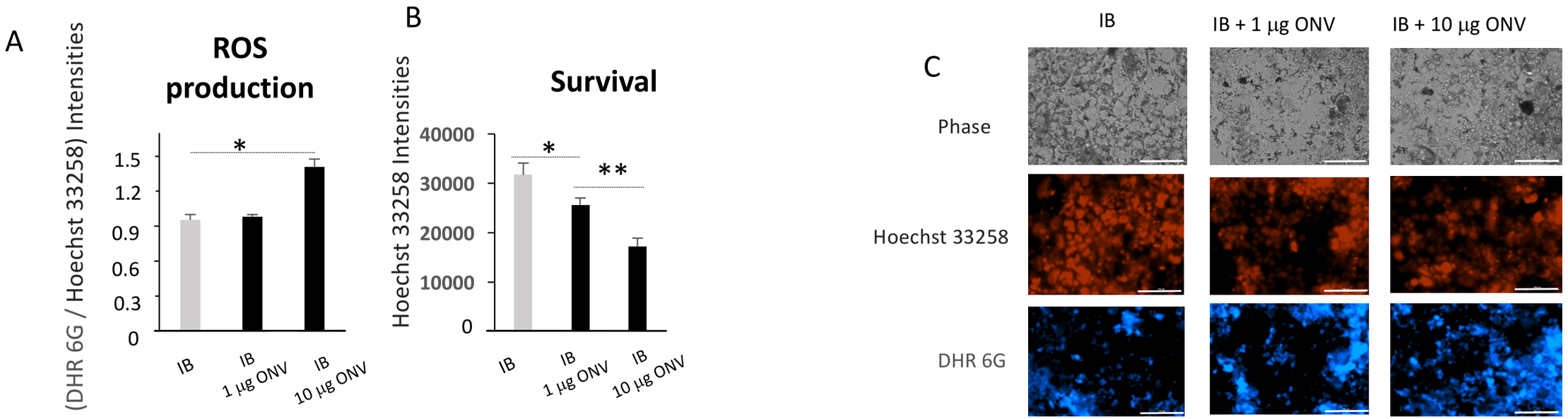

Figure S3: (A) Reactive oxygen species (ROS) production (DHR 6G fluorescence) in IB treated with different ONV concentrations. (B) Quantification of cell death in IB treated with different quantities of ONV.
Results represent Hoescht 33258 fluorescence intensities. (C) Representative images used to quantify the number of nuclei (Hoescht 33258 fluorescence) and the ROS production (DHR 6G fluorescence) in the IB treated with ONV. Bar=100µm.

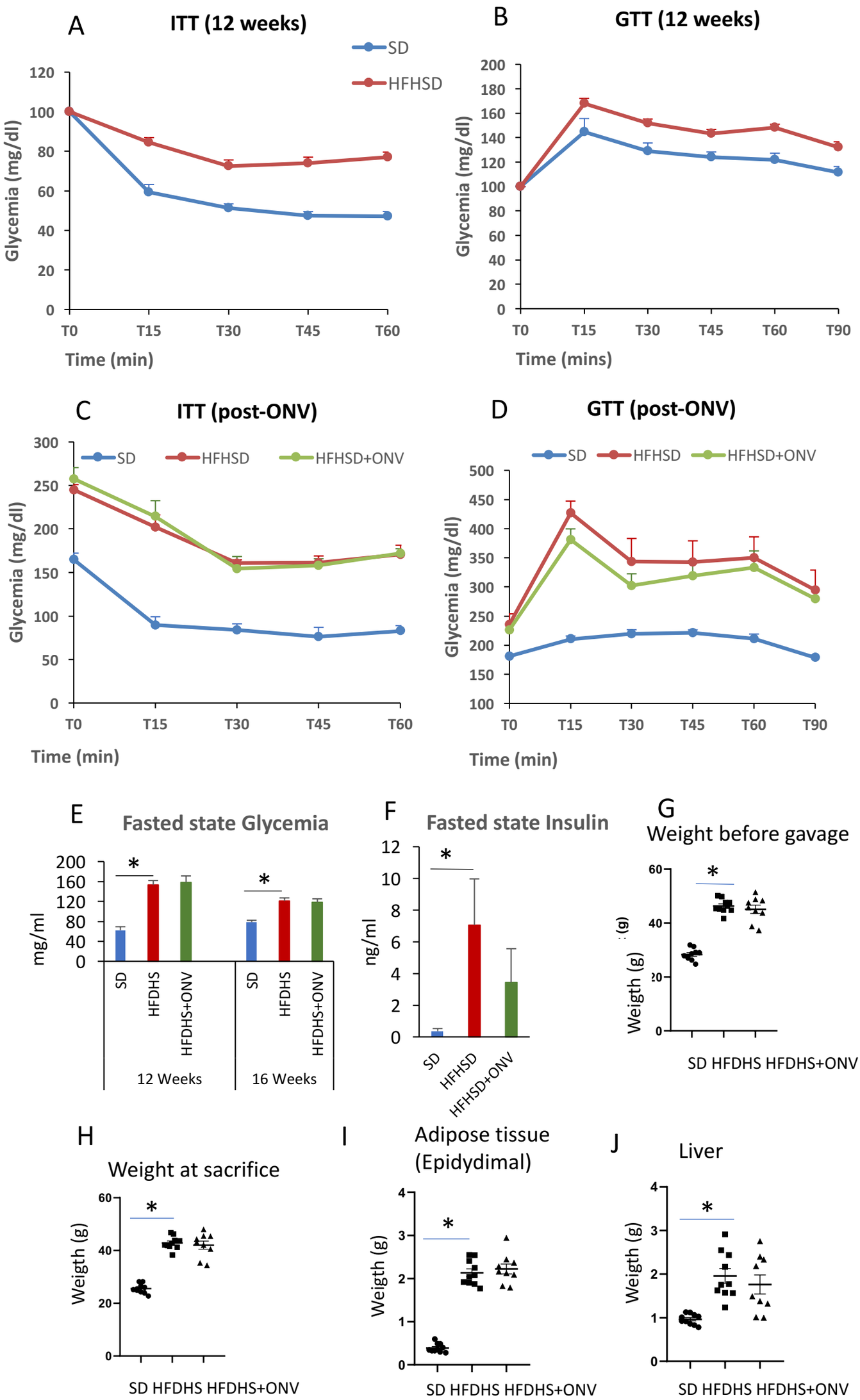

Figure S4: ONV effects in DIO mice. (A) Insulin tolerance test and (B) Glucose tolerance test at 12 weeks before the gavage with ONV (n=10). (C) Insulin tolerance test and (D) Glucose tolerance test after one month of gavage with 150µg ONV (n=5). (E) Glycemia before and after gavage (n=10), (F) Plasma insulin after gavage (n=3), (G and H) body weight before and after gavage (n=10). (I) Epidydimal adipose tissue weight at sacrifice (n=10), (J) Liver weight at sacrifice (n=10).